

A Monte Carlo study of capillary condensation of krypton within realistic models of templated mesoporous silica materials

Francisco R. Hung^a, Benoit Coasne^{a,†}, Keith E. Gubbins^a, Flor R. Siperstein^b and Malgorzata Sliwinska-Bartkowiak^c

^a Center for High Performance Simulation and Department of Chemical and Biomolecular Engineering, North Carolina State University, Raleigh, NC 27695-7905, USA

^b Departament d'Enginyeria Quimica, Universitat Rovira i Virgili, Campus Sescelades, Avenida dels Països Catalans 26, 43007, Tarragona, Spain

^c Institute of Physics, Adam Mickiewicz University, Umultowska 85, 61-614 Poznan, Poland

1. ABSTRACT

We report molecular simulations of Kr adsorption at 87 and 100 K in three atomistic silica mesopores with an average pore diameter of 6.4 nm: (a) a pore that keeps the morphological features of a MCM-41 mesoscale model, generated from lattice Monte Carlo simulations mimicking its fabrication process; (b) a smooth, regular cylindrical pore; and (c) a cylindrical pore with constriction. Surface roughness and structural defects significantly affect Kr adsorption: marked differences were observed in the adsorption isotherms, isosteric heat curves and pore filling mechanisms for the three pore models. Our results suggest that the molecular-level surface disorder for the first pore model is too high, but its roughness at larger length scales (10-50 Å), as determined from simulated SANS spectrum, is in agreement with experimental results. The dense phase of Kr inside the three pore models exhibits a liquid-like global structure, even though the temperatures considered are well below the bulk triple point.

2. INTRODUCTION

Templated mesoporous silica material MCM-41 [1] consists of hexagonal arrays of cylindrical pores with diameters between 1.5 and 20 nm, narrow pore size distributions and negligible pore networking. These properties make these materials ideal for fundamental studies aimed at determining the effect of surface forces, confinement and reduced dimensionality on the phase behavior of host molecules. The features of MCM-41 materials [2] make them suitable for a number of applications in catalysis, adsorption, optics, as low dielectric constant materials to insulate integrated circuits, and as host materials for polymers, nanoparticles and enzymes [2]. The gas-liquid transition of adsorbates in templated mesoporous silica materials has been extensively studied by experiment, theory and molecular simulation [3]. From a molecular simulation viewpoint, a number of silica pore models have

[†] Present address: Laboratoire de Physicochimie de la Matière Condensée (UMR CNRS 5617), Université de Montpellier II, Place Eugène Bataillon, 34095 Montpellier, Cedex 5, France.

been used recently [4-7] to study adsorption of different pure substances and mixtures on MCM-41 type materials. Most of these pore models exhibit a regular cylindrical geometry, but it is unclear whether those models are realistic representations of MCM-41, due to the lack of conclusive experiments regarding its pore surface roughness and morphology. Some experimental results [8,9] attribute some surface roughness to the pore walls, whereas others [10,11] suggest a smooth surface at molecular scales (3-7 Å), with roughness and other morphological defects (constrictions, tortuosity) at larger length scales (20-50 Å).

One possible approach to modeling porous solids is to mimic the synthesis process of the real material using simulations, a strategy used in the past [12] to develop realistic models for Vycor and controlled pore glasses (CPG). Recently, Siperstein and Gubbins [13] used lattice Monte Carlo simulations to study the behavior of surfactant-inorganic oxide-solvent systems and mimic the synthesis of templated mesoporous silica materials. Low values of the surfactant/inorganic oxide concentration ratio led to formation of hexagonally ordered porous structures resembling that of MCM-41 material. Pores with an important degree of surface roughness and structural defects were obtained from this mesoscale simulation protocol. Recently, Coasne *et al.* [14,15] developed a fully-atomistic model based on the morphological features of this mesoscale model. In doing this “downscaling” process, atomic details can be included, more accurate potentials can be used for the adsorbate-wall interactions, and the effect of structural defects on the adsorbate phase behavior can be assessed. In this paper we summarize our methodology used to generate atomistic silica mesopores. Three pore models were considered in this study: 1) a pore that keeps the morphological features of the mesoscale model of Siperstein and Gubbins [13]; 2) a pore with regular cylindrical shape; and 3) a cylindrical pore with constrictions. We performed Grand Canonical Monte Carlo (GCMC) simulations of krypton adsorption at 100 K and 87 K, for which we report adsorption isotherms and isosteric heats of adsorption. Kr adsorption at low temperatures (77, 87 K) has been used in the past for characterization of porous materials with very low surface areas and volumes [16,17]. We discuss the effect of surface roughness and structural defects, and we compare with experimental results available in the literature. Similar results for argon and xenon on atomistic silica mesopores have been presented in other publications [14,15].

2. SIMULATION DETAILS

A detailed description of the simulation protocol used to generate and characterize atomistic silica mesopores has been reported elsewhere [14,15]. Similarly, the mimetic simulation procedure to obtain mesoscale, lattice models of MCM-41 type materials has been described in detail in previous publications [13]. The lattice positions of the inorganic oxide segments from the mimetic simulations were scaled to obtain a material with a pore diameter $D = 6.4$ nm and a length $L = 28$ nm. We isolated one of these pores and carved out its morphology from an atomistic box with a number of unit cells of cubic cristoballite. Following that, silicon atoms that are in an incomplete tetrahedral environment are removed, as well as oxygen atoms with two dangling bonds; oxygen atoms with one dangling bond are saturated with hydrogen atoms. This procedure ensures that all silicon atoms have no dangling bonds, all oxygen atoms have at least one saturated bond with a silicon atom, the atomistic simulation box has no net electrical charge and the pore surface is modeled in a realistic way. To mimic an amorphous silica surface, all the O, Si and H atoms were slightly displaced a random distance, and in a final step, the structure was further relaxed by performing a NVT Monte Carlo simulation using suitable potentials and parameters [15]. The generated atomistic silica mesopore (model A) has an average pore radius of 3.2 nm with a dispersion of

± 1 nm, and its roughness at length scales between 10 Å and 50 Å was determined from simulated small angle neutron scattering spectra (SANS) [15]. This procedure to generate atomistic silica pores was originally proposed by Pellenq and Levitz [18] to model Vycor glass. We used a similar simulation protocol to generate two additional silica pores: a regular cylindrical pore with $D = 6.4$ nm (model B), and a cylindrical pore of diameter $D = 8.2$ nm with a constriction of $D = 4.1$ nm (model C). Similar constricted pores were considered in previous simulation studies [5,7,19,20]. The dimensions of pore model C are such that model B is an equivalent regular cylindrical pore with the same length, volume, and on average, the same degree of confinement. Both pore models B and C have a length of 15 nm, and periodic boundary conditions were applied in the axial direction for all three pore models. A schematic of the procedure used to generate the atomistic pores, as well as front views and cross sections of the three pore models used in this study are shown in Fig. 1.

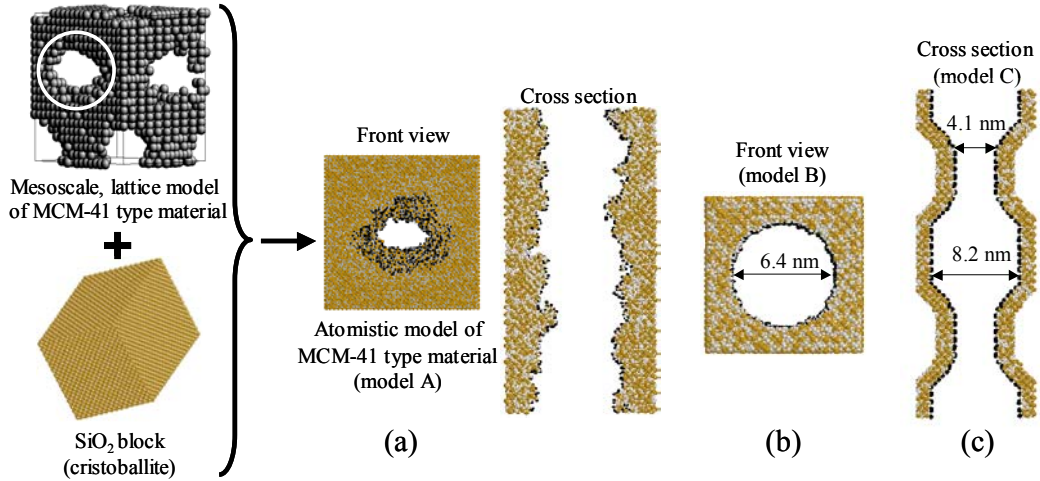


Fig. 1. Scheme of the procedure used to generate atomistic silica pore models used in this study. Front views and/or cross sections of the three pore models are also shown. Oxygen, silicon and hydrogen atoms are depicted in white, grey and black, respectively. For model C, we have represented two simulation boxes aligned in the axial direction z .

Krypton was modeled as a Lennard-Jones (LJ) fluid with parameters taken from Ref. [18]: $\sigma_{ff} = 0.369$ nm, $\varepsilon_{ff}/k_B = 170$ K. The interaction of Kr atoms with O, Si and H atoms in the substrate was modeled using the PN-TraZ potentials and parameters [18]. We performed Grand Canonical Monte Carlo (GCMC) simulations of Kr adsorption at $T = 100$ K and 87 K. The ideal gas equation and the properties of the LJ fluid at coexistence [21] were used to calculate chemical potentials μ from relative pressures P/P_0 . To speed up our simulation runs, we have used an energy grid [18] with an elementary cube size of about 1 \AA^3 to compute the adsorbate-wall potential energy. Thermodynamic properties were averaged over a minimum of 10^5 MC steps per particle (typical systems had up to 15000 particles); however, much longer runs were considered near the phase transitions. We also determined the isosteric heat of adsorption q_{st} [22], the local density profile ρ and the “renormalized” 3D positional pair correlation function $g(R)$ (where R is the in-pore distance) following the procedure reported in our previous work [23].

3. RESULTS

Kr adsorption isotherms are presented in Fig. 2 for the three atomistic silica mesopore models. The adsorbed amounts were normalized with respect to the quantity of adsorbate when each

pore is filled. At a fixed T , the adsorption curves exhibit different features and are significantly affected by the pore morphology. For pore model B there is one vertical jump due to capillary condensation, whereas two discontinuities were observed for model C. The adsorption isotherm for pore model A also exhibits two small jumps that are not as sharp as those observed in models B and C. The surface area of pore model A is larger than that of model C, which in turn is larger than that of model B. In addition, pore model A exhibits an important degree of surface roughness and therefore there are more sites where molecules can get preferentially adsorbed. These factors cause pore model A to exhibit a lower capillary condensation pressure, a larger value of N/N_0 at any given P/P_0 , and an adsorption curve that looks smoother than those for the other pore models. Pore model C fills at a lower value of P/P_0 than model B, and at a fixed value of P/P_0 , model C exhibits a larger value of N/N_0 than that for model B. Pore model A shows an asymmetrical hysteresis loop, which is typical of adsorption on materials with interconnected pores, e.g. Vycor [7,12,18], but were also observed in unconnected pores with morphological defects [5,7].

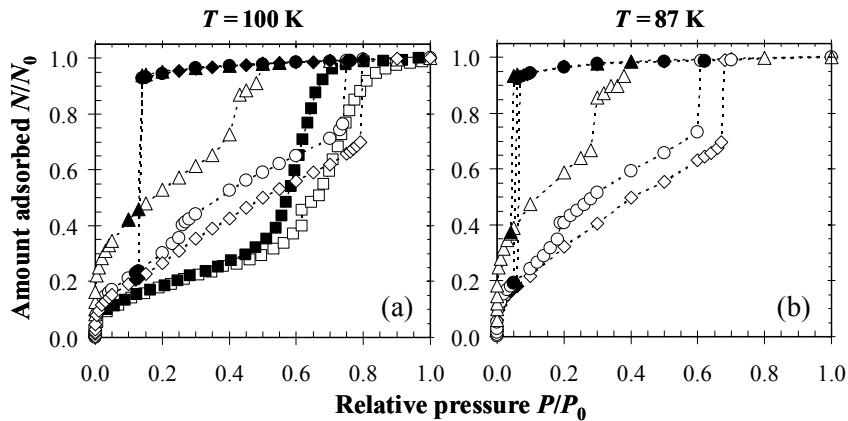


Fig. 2. Adsorption-desorption isotherms for Kr at (a) $T = 100$ K, and (b) $T = 87$ K. Results for pore models A, B and C are depicted by triangles, diamonds and circles, respectively; squares represent experimental results on SBA-15 with a similar mean pore diameter (6.4 nm) [24]. Open and closed symbols represent adsorption and desorption, respectively.

Evaporation takes place approximately at the same value of P/P_0 in the three pore models. Due to the use of periodic boundary conditions, there is no interface with the bulk and evaporation occurs via nucleation of a gas bubble (cavitation) in the center of the pore. The mean pore sizes in term of Kr molecular diameters ($\sigma_{\text{Kr}} = 0.369$ nm) are such that the desorption process does not seem to be affected by the pore morphology. Our adsorption-desorption simulation study of Ar ($\sigma_{\text{Ar}} = 0.34$ nm) on pore model A [15] shows a desorption curve similar to that of Kr, but for Xe ($\sigma_{\text{Xe}} = 0.410$ nm) it was found that the desorption curve is composed of reversible paths and two small jumps in the adsorbed amount [14,15]. Moreover, for Ar adsorption-desorption on cylindrical pores of $D = 6.0$ nm with a constriction of $D = 4.0$ nm [7], the isotherms exhibit the same features observed in this study for Kr on pore model C; however, for Ar on cylindrical pores of $D = 5.0$ nm with a constriction of $D = 2.5$ nm [25], a two-step desorption process was observed. These results suggest that the desorption mechanism in pores with morphological defects strongly depends on pore geometry and adsorbate size. For a given pore model, as temperature increases the amount adsorbed at a certain value of P/P_0 decreases, capillary condensation and evaporation take place at higher values of P/P_0 , the hysteresis loop shrinks, and the jumps in the adsorption isotherms are less marked.

In Fig. 2 we also compare our simulation results at 100 K with experiments for SBA-15 with the same mean pore diameter (6.4 nm) from Morishige *et al.* [24]. The shape of the experimental adsorption isotherm resembles that of pore model A, and the step due to capillary condensation is steep but not vertical. This can be due to the presence of a pore size distribution, as well as morphological and topological features (changes in pore shape, surface roughness, energetic heterogeneity, microporosity, interconnected pores). On the other hand, the experimental capillary condensation pressure is similar to what was obtained for pore model B, and N/N_0 is overestimated by all pore models. The lack of quantitative agreement between simulations and experiments could be due, at least, to two reasons. First, the intermolecular potential adsorbate-wall can be overestimating the attractive energy: for simulated Ar adsorption in regular cylindrical silica pores, it has been reported that a reduction of 3% in selected parameters can lead to quantitative agreement in film thickness (t -plot) with experimental results [7]. Second, the degree of surface disorder for pore model A is too high at the molecular level, leading to overestimation of N/N_0 and underestimation of the capillary condensation pressure. These conclusions are corroborated by our results for the isosteric heat of adsorption q_{st} for Kr at 100 K, which are presented in Fig. 3. The experimental value of q_{st} at low coverages is 15 kJ/mol [18], in agreement with results for pore models B and C. At low pore filling fractions ($N/N_0 < 0.3$), q_{st} for pore model A largely overestimates the values of models B and C [Fig. 3(a)], since the adsorbate-wall contribution to q_{st} for pore model A is significantly larger than those for the other pore models [Fig. 3(b)]. This explains why N/N_0 at a given pressure prior to capillary condensation is much larger for pore model A, and suggests that the degree of surface disorder for pore model A is too high at the molecular level. This conclusion is also supported by our results for Ar and Xe adsorption [14,15] and their comparison with available experimental data. Nevertheless, simulated SANS results for pore model A [15] indicates that its roughness at length scales between 10 Å and 50 Å is in agreement with experimental measurements for MCM-41 type materials [10,11].

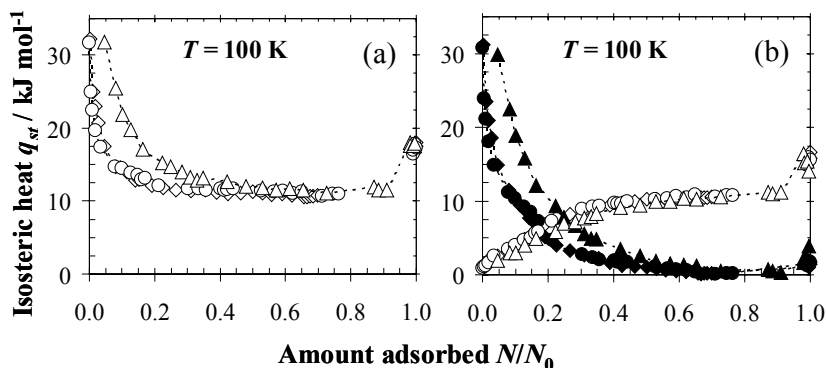
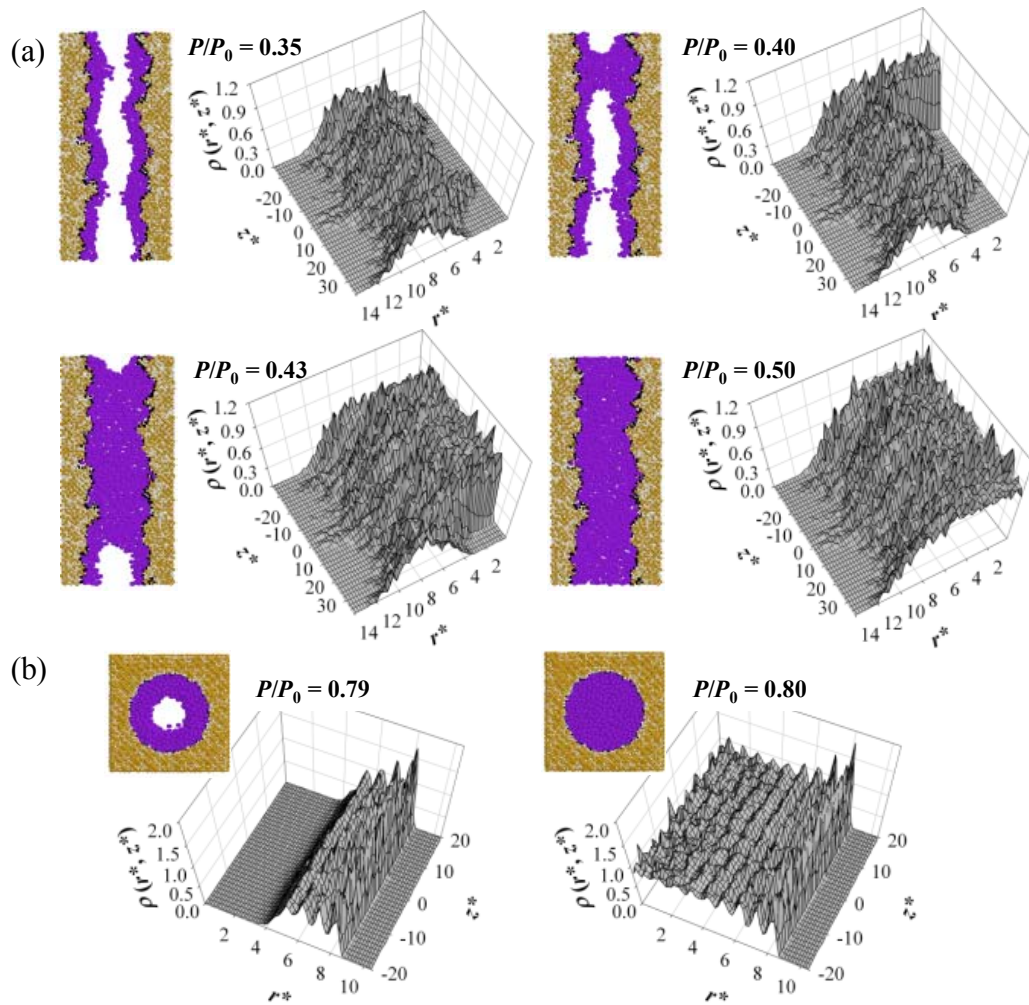


Fig. 3. Isosteric heat of adsorption q_{st} as a function of coverage fraction N/N_0 , for Kr adsorption on atomistic silica mesopores at 100 K: (a) total q_{st} , and (b) adsorbate-wall (filled symbols) and adsorbate-adsorbate (open symbols) contributions to q_{st} . Symbols as in Fig. 2.

We have used our pore models to discuss the effect of surface roughness and structural defects on the adsorption mechanism and on the nature of the dense phases. In Fig. 4 we present plots of the local density profile $\rho(r, z)$, as well as representative simulation snapshots for the three pore models at different values of P/P_0 and $T = 100$ K. For pore model A, ρ also depends on the angular coordinate θ ; nevertheless, a plot of $\rho(r, z)$ can provide a suitable measure of the local state of the confined phase. As P/P_0 increases, the pore walls are covered by an adsorbate film whose thickness increase gradually with P/P_0 , until it reaches a point when there is formation of a condensate “bridge” between low density regions of adsorbate in

the center of the pore [$P/P_0 = 0.40$, Fig. 4(a)]. Most of the low density regions condense suddenly at $P/P_0 = 0.43$ [Fig. 4(a)], which is also signaled by a jump in the adsorption isotherm (Fig. 2). Finally, at $P/P_0 = 0.50$ the pore is filled with a condensed phase and a smaller jump in the isotherm is also observed (Fig. 2). A similar behavior has been observed in past studies for adsorbents with distinct chemical and morphological heterogeneities [7,18-20,26-28], and is similar to the filling mechanism observed for the constricted pore [Fig. 4(c)]. As P/P_0 increases, we see again an increase in the adsorbed film thickness until it becomes unstable and condensation takes place in the constrictions [$P/P_0 = 0.26$, Fig. 4(c)]. The size of the constriction ($D = 4.1$ nm) is comparable to the diameter at the narrowest part of pore model A ($D = 5.4$ nm), where the liquid-like “bridge” first forms [$P/P_0 = 0.40$, Fig. 4(a)]. This leads to the formation of hemispherical gas-liquid interfaces that coexist with condensed regions, as it was observed for pore model A. These gas-like regions slightly shrink as P/P_0 increases, until the main cavity is suddenly filled with a condensed phase [Fig. 4(c)]. The adsorption isotherm also exhibits two jumps when these condensation processes take place (Fig. 2). In contrast, for pore model B [Fig. 4(b)], the adsorbed film thickness increases with P/P_0 until it reaches its stability limit [$P/P_0 = 0.79$, Fig. 4(b)]. A slight increase in P/P_0 makes the pore to be suddenly filled with a condensed phase and a vertical jump is observed in the adsorption isotherm [Fig. 4(b) and Fig. 2]. The adsorption mechanisms at $T = 87$ K for the three pore models are similar to those described at $T = 100$ K.



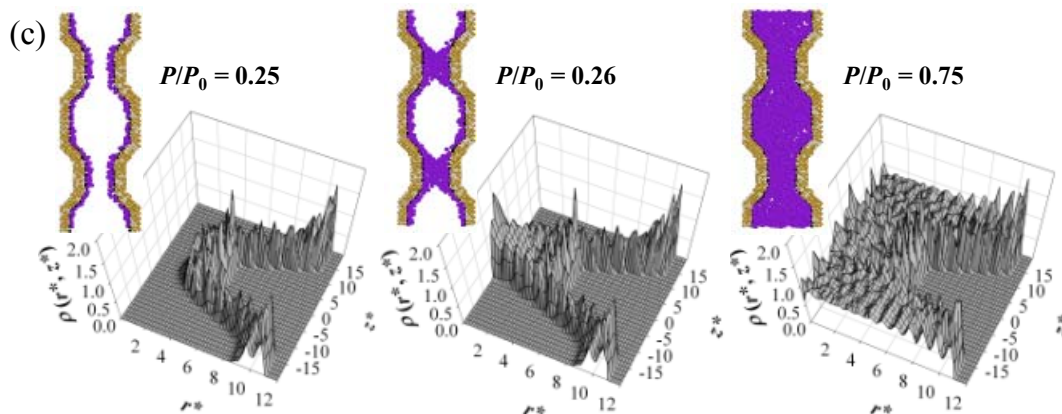


Fig. 4. Local density profile $\rho(r, z)$, and front views or cross sections of representative simulation snapshots of the confined phase inside (a) pore model A, (b) pore model B, and (c) pore model C, for different values of P/P_0 at $T=100$ K. Two simulation boxes aligned in the axial direction z are represented in the snapshots for pore model C, to help visualization of the confined phase features.

In Fig. 5 we show the 3D positional pair correlation function $g(R)$ for Kr inside the three pore models at $T=87$ K and $P/P_0=1$. These functions suggest that the three pore models are filled with dense Kr with a liquid-like structure, even though the temperature is well below the bulk triple point (116 K). The maximum in the first peak of $g(R)$ is slightly larger for pore model B as compared to the other models, with Kr inside pore model A exhibiting the lowest value for this first peak. An investigation of the global and local structure of Kr freezing within these pores is currently in progress.

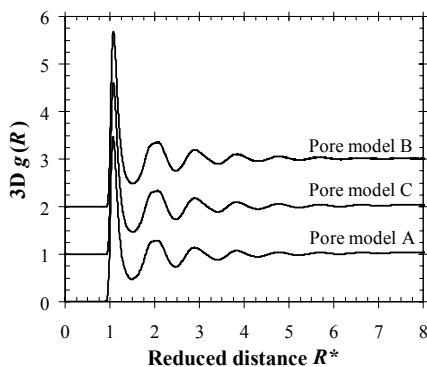


Fig. 5. 3D positional pair correlation function $g(R)$ for Kr at $T=87$ K and $P/P_0=1$.

4. CONCLUSIONS

We performed GCMC simulations of Kr adsorption on three atomistic silica mesopores: (a) a pore (model A) that keeps the morphological features of the MCM-41 mesoscale model of Siperstein and Gubbins [13]; (b) a regular cylindrical pore (model B); and (c) a cylindrical pore with constriction (model C). Adsorption isotherms, isosteric heats, density profiles and 3D positional pair correlation functions were obtained at $T=100$ K and 87 K, below the bulk triple point of Kr (116 K), and compared with experimental data. Our results suggest that the degree of surface disorder for pore model A is too high at the molecular level. However, simulated SANS spectrum shows that its roughness at larger length scales (10-50 Å) is in agreement with MCM-41 experimental results [10,11]; a detailed account of these results are presented in ref. 15. We are currently improving our pore model A so that its molecular

roughness agrees with experimental data. Surface roughness and structural defects significantly affect Kr adsorption: marked differences were observed in the adsorption isotherms, isosteric heat curves and pore filling mechanisms. The dense phase of Kr inside the three pore models exhibit a liquid-like global structure; a detailed investigation of the freezing behavior of Kr within these pores is currently in progress.

We are grateful to R. J.-M. Pellenq (CNRS-Marseille) for helpful discussions. This work was supported by grants from NSF (CTS-0211792), KBN (2P03B 014 24) and NATO (PST.CLG.978802). This research used supercomputing resources from HPC-NCSU, SDSC (NSF/MRAC CHE050047S) and NERSC (DOE DE-FGO2-98ER14847).

REFERENCES

- [1] C. T. Kresge, M. E. Leonowicz, W. J. Roth, J. C. Vartuli and J. S. Beck, *Nature*, 359 (1992) 710.
- [2] For recent reviews, see P. Selvam, S. K. Bhatia and C. G. Sonwane, *Ind. Eng. Chem. Res.*, 40 (2001) 3237; G. J. de A. A. Soler-Illia, C. Sanchez, B. Lebeau and J. Patarin, *Chem. Rev.*, 102 (2002) 4093; F. Schüth and W. Schmidt, *Adv. Mater.*, 14 (2002) 629.
- [3] For a review, see L. D. Gelb, K. E. Gubbins, R. Radhakrishnan and M. Sliwinska-Bartkowiak, *Rep. Prog. Phys.*, 62 (1999) 1573.
- [4] M. W. Maddox, J. P. Olivier and K. E. Gubbins, *Langmuir*, 13 (1997) 1737.
- [5] B. Coasne, A. Grosman, C. Ortega and R. J. M. Pellenq, *Studies in Surface Science and Catalysis*, 144 (F. Rodríguez-Reinoso, B. McEnaney, J. Rouquerol and K. Unger, eds.), Elsevier, Amsterdam (2002) 35.
- [6] Y. He and N. A. Seaton, *Langmuir*, 19 (2003) 10132.
- [7] B. Coasne and R. J.-M. Pellenq, *J. Chem. Phys.*, 121 (2004) 3767; 120 (2004) 2913.
- [8] V. B. Fenelonov, A. Y. Derevyankin, S. D. Kirik, L. A. Solovyov, A. N. Shmakov, J.-L. Bonardet, A. Gedeon and V. N. Romannikov, *Micropor. Mesopor. Mat.*, 44-45 (2001) 33.
- [9] A. Berenguer-Murcia, J. García-Martínez, D. Cazorla-Amorós, A. Martínez-Alonso, J. M. D. Tascón and A. Linares-Solano, *Studies in Surface Science and Catalysis*, 144 (F. Rodríguez-Reinoso, B. McEnaney, J. Rouquerol and K. Unger, eds.), Elsevier, Amsterdam (2002) 83.
- [10] K. J. Edler, P. A. Reynolds and J. W. White, *J. Phys. Chem. B*, 102 (1998) 3676.
- [11] C. G. Sonwane, S. K. Bhatia and N. J. Calos, *Langmuir*, 15 (1999) 4603.
- [12] L. D. Gelb and K. E. Gubbins, *Langmuir*, 14 (1998) 2097; *Mol. Phys.*, 96 (1999) 1795.
- [13] F. R. Siperstein and K. E. Gubbins, *Mol. Sim.*, 27 (2001) 339; *Langmuir*, 19 (2003) 2049.
- [14] B. Coasne, F. R. Hung, F. R. Siperstein and K. E. Gubbins, *Ann. Chim-Sci. Mat.*, in press (2005).
- [15] B. Coasne, F. R. Hung, R. J.-M. Pellenq, F. R. Siperstein and K. E. Gubbins, *Langmuir*, submitted (2005).
- [16] S. J. Gregg and K. S. W. Sing, *Adsorption, Surface Area and Porosity*, 2nd edition, Academic Press, London, 1982.
- [17] T. Takei and M. Chikazawa, *J. Ceram. Soc. Jpn.*, 106 (1998) 353.
- [18] R. J.-M. Pellenq and P. E. Levitz, *Mol. Phys.*, 100 (2002) 2059.
- [19] L. Sarkisov and P. A. Monson, *Langmuir*, 17 (2001) 7600.
- [20] A. Vishnyakov and A. V. Neimark, *Langmuir*, 19 (2003) 3240.
- [21] R. Agrawal and D. A. Kofke, *Mol. Phys.*, 85 (1995) 43.
- [22] D. Nicholson and N. G. Parsonage, *Computer Simulation and the Statistical Mechanics of Adsorption*, Academic Press, London, 1982.
- [23] F. R. Hung, B. Coasne, K. E. Gubbins, E. E. Santiso, F. R. Siperstein and M. Sliwinska-Bartkowiak, *J. Chem. Phys.*, 122 (2005) 144706.
- [24] K. Morishige, K. Kawano and T. Hayashigi, *J. Phys. Chem. B.*, 104 (2000) 10298.
- [25] B. Coasne, K. E. Gubbins and R. J.-M. Pellenq, *Part. Part. Syst. Character.*, 20 (2004) 1.
- [26] H. Bock and M. Schoen, *Phys. Rev. E*, 59 (1999) 4122.
- [27] J. Puibasset, *J. Chem. Phys.*, 122 (2005) 134710.
- [28] F. Detcheverry, E. Kierlik, M. L. Rosinberg, and G. Tarjus, *Phys. Rev. E*, 68 (2003) 061504.